

Communication

## Product Selectivity Controlled by Zeolite Crystals in Biomass Hydrogenation over a Palladium Catalyst

Chengtao Wang, Liang Wang, Jian Zhang, Hong Wang, James P. Lewis, and Feng-Shou Xiao

*J. Am. Chem. Soc.*, **Just Accepted Manuscript** • DOI: 10.1021/jacs.6b04951 • Publication Date (Web): 16 Jun 2016

Downloaded from <http://pubs.acs.org> on June 20, 2016

### Just Accepted

"Just Accepted" manuscripts have been peer-reviewed and accepted for publication. They are posted online prior to technical editing, formatting for publication and author proofing. The American Chemical Society provides "Just Accepted" as a free service to the research community to expedite the dissemination of scientific material as soon as possible after acceptance. "Just Accepted" manuscripts appear in full in PDF format accompanied by an HTML abstract. "Just Accepted" manuscripts have been fully peer reviewed, but should not be considered the official version of record. They are accessible to all readers and citable by the Digital Object Identifier (DOI®). "Just Accepted" is an optional service offered to authors. Therefore, the "Just Accepted" Web site may not include all articles that will be published in the journal. After a manuscript is technically edited and formatted, it will be removed from the "Just Accepted" Web site and published as an ASAP article. Note that technical editing may introduce minor changes to the manuscript text and/or graphics which could affect content, and all legal disclaimers and ethical guidelines that apply to the journal pertain. ACS cannot be held responsible for errors or consequences arising from the use of information contained in these "Just Accepted" manuscripts.



ACS Publications

# Product Selectivity Controlled by Zeolite Crystals in Biomass Hydrogenation over a Palladium Catalyst

Chengtao Wang,<sup>a</sup> Liang Wang,<sup>\*,a</sup> Jian Zhang,<sup>a</sup> Hong Wang,<sup>b</sup> James P. Lewis,<sup>b</sup> and Feng-Shou Xiao<sup>\*,a,c</sup>

<sup>a</sup> Key Lab of Applied Chemistry of Zhejiang Province, Department of Chemistry, Zhejiang University, Hangzhou 310028, China.

<sup>b</sup> Department of Physics, West Virginia University, Morgantown, WV 26506-6315, USA.

<sup>c</sup> Key Lab of Biomass Chemical Engineering of Ministry of Education, Zhejiang University, Hangzhou 310027, China.

**KEYWORDS.** Zeolite; Core-shell structure; Pd nanoparticle; Furfural; Biomass hydrogenation

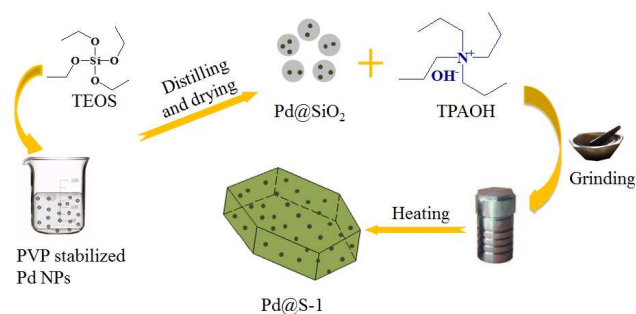
**ABSTRACT:** This work delineates first example for controlling product selectivity in metal-catalyzed hydrogenation of biomass by zeolite crystals. The key to this success is to combine the advantages of both Pd nanoparticles (highly active sites) and zeolite micropores (controllable diffusion of reactants and products), which was achieved from encapsulation of the Pd nanoparticles inside of Silicalite-I zeolite crystals as a core-shell structure (Pd@S-1). In the hydrogenation of biomass-derived furfural, the furan selectivity over the Pd@S-1 is as high as 98.7%, outperforming the furan selectivity (5.6%) over conventional Pd nanoparticles impregnated with S-1 zeolite crystals (Pd/S-1). The extraordinary furan selectivity in the hydrogenation over the Pd@S-1 is reasonably attributed to the distinguishable mass transfer of the hydrogenated products in the zeolite micropores.

Selective transformation of renewable biomass-derived feedstocks plays a key role in sustainable production of bio-fuels and fine chemicals.<sup>1-10</sup> Up to now, many economically viable processes have been developed for the conversion of biomass.<sup>6-10</sup> For example, pyrolysis or hydration of lignin and cellulose, which contain more than 30% of the organic carbon on earth, to produce various platform chemicals of phenols, levulinic acids, and furfurals has been deemed to be promising alternatives to crude oil.<sup>11-15</sup> In these processes, it is notable that the biomass derived chemicals normally have relatively high oxygen content, which strongly limits their applications.<sup>11-13</sup> Therefore, upgrading the biomass-derived chemicals by hydrogenation to selectively remove the oxygen groups in the chemicals is strongly desirable. However, it still has a challenge to control the product selectivity in biomass hydrogenation yet because these reaction pathways with many undesirable reactions are very complex.

The transition metal nanoparticles have been widely applied in the hydrogenation of biomass.<sup>16-19</sup> In these cases, it is not easy to control the product selectivity because the hydrogenation directly occurs on the exposed metal active sites. On the other hand, it is well known that the mass transfer in catalytic conversion of hydrocarbons is very sensitive to the product selectivity.<sup>20-23</sup> Typically, introduction of mesoporosity in zeolite crystals and modification of catalyst wettability significantly change the diffusion of reac-

tants and products,<sup>21-23</sup> finally enhancing the product selectivity in catalytic conversion. However, rare efficient strategies exist so far, which allows for rationally controlling the diffusion of reactants and products in metal-catalyzed hydrogenations.

Here we report a generalized strategy for preparation of excellently selective and highly active catalysts by encapsulation of metal nanoparticles inside of microporous silicalite-I (S-1) zeolite as core-shell structures (metal@zeolite), where the metal nanoparticles serve as catalytically active sites and the zeolite micropores control the product selectivity by changing molecular diffusion. Considering that Pd nanoparticles are highly active but poor selective in the biomass hydrogenation and S-1 zeolite is easily synthesized, a Pd@S-1 was successfully prepared from solvent-free crystallization of a solid mixture including Pd nanoparticles, amorphous silica, and organic structural directing agent (OSDA).<sup>24</sup> As expected, the Pd@S-1 is highly active and excellently selective in the hydrogenation of biomass derived furfural, giving furan selectivity as high as 98.7% with furfural conversion of 91.3%. In contrast, conventional supported catalysts show relatively low furan selectivities, which are due to the complexity of reactive pathways and difficulty in controlling the selectivity (Scheme S1).



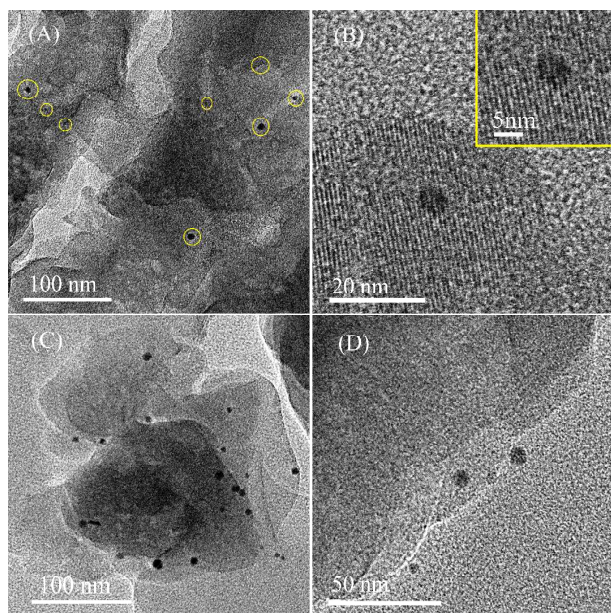
**Scheme 1.** Synthesis of Pd@S-1 catalyst.

Scheme 1 shows procedure for synthesis of the Pd@S-1. At first, the Pd nanoparticles was encapsulated with amorphous SiO<sub>2</sub> obtained from controllable hydrolysis of tetraethyl orthosilicate (TEOS) in polyvinyl pyrrolidone (PVP) stabilized Pd nanoparticle solution, followed by addition of

1 tetrapropyl ammonium hydroxide (TPAOH) solution. After  
2 grinding at room temperature in air, the solid mixture was  
3 transferred into an autoclave for crystallization at 180 °C for  
4 3 days. After washing with water, drying at 100 °C, and calcin-  
5 ing at 550 °C for 4 h, the Pd@S-1 was finally obtained.  
6 The Pd loading was calculated at 0.34% by ICP analysis. For  
7 comparison, the Pd nanoparticles supported on S-1 and  
8 Al<sub>2</sub>O<sub>3</sub> by impregnation method were denoted as Pd/S-1 and  
9 Pd/Al<sub>2</sub>O<sub>3</sub> with similar Pd loadings at 0.33% and 0.31%, res-  
10 pectively.

11 It is worth mentioning that the solvent-free crystallization  
12 plays a critical role for the successful preparation of Pd@S-1,  
13 which offers a possibility to fully encapsulate the Pd nano-  
14 particles inside of S-1 single crystals. If the Pd nanoparticles  
15 are directly exposed to external surface of the catalysts pre-  
16 pared from other routes such as conventional hydrothermal  
17 synthesis of zeolites, the product selectivity in the biomass  
18 hydrogenation should be reduced significantly.

19 Figure S1 shows XRD patterns of various samples. The  
20 Pd@S-1 and Pd/S-1 exhibit XRD peaks associated with typi-  
21 cal MFI zeolite structure. Notably, it is difficult to observe  
22 the peaks associated with metallic Pd crystals, indicating  
23 high dispersion and low loading of Pd nanoparticles on/in  
24 the samples. Figure S2 shows N<sub>2</sub> sorption isotherms of the  
25 S-1, Pd@S-1, and Pd/S-1 samples. They give high surface  
26 areas (BET 346-450 m<sup>2</sup>/g) and large pore volumes (0.14-  
27 0.18 m<sup>3</sup>/g, Table S1), indicating the successful formation of  
28 zeolite crystals.



29 **Figure 1.** Tomogram-section TEM images of (A and B) the  
30 Pd@S-1 and (C and D) Pd/S-1. Insert in B: Enlarged view.

31 Figure 1 shows tomogram-section transmission electron  
32 microscopy (TEM) tomography images of the Pd@S-1 and  
33 Pd/S-1. This technology could offer the sectioned view of the  
34 sample, thus avoiding the influence of metal nanoparticles  
35 on the external surface. In the Pd@S-1, the Pd nanoparticles  
36 could be directly observed (Figure 1A), confirming these  
37 nanoparticles are indeed encapsulated within the S-1 zeolite  
38 crystals as the core-shell structure. It is shown that the size  
39 of Pd nanoparticles in the Pd@S-1 is ranged of 3.7-11.7 nm  
40 with a mean size at 6.9 nm (Figure S3A). In the sectioned  
41 view of the Pd/S-1, the Pd nanoparticles are found only on  
42 the side of S-1 crystals, indicating that the Pd nanoparticles  
43 are located only on the external surface of the S-1 crystals.

44 By counting more than 100 nanoparticles, the nanoparticle  
45 size of the Pd/S-1 is calculated at 4.1-10.9 nm (Figure S3B),  
46 which is similar to those of the Pd@S-1 and Pd/Al<sub>2</sub>O<sub>3</sub> (Fig-  
47 ures S3A and S4).

48 Furthermore, the structure of the Pd@S-1 was investigat-  
49 ed by hydrogenation of probing molecules such as benzal-  
50 dehyde (BA) and 3,5-isopropylbenzaldehyde (DPBA) with  
51 different molecular diameter. Table S2 present the catalytic  
52 data in the hydrogenation of mixed substrates of BA and  
53 DPBA over the Pd@S-1, Pd/S-1, and Pd/Al<sub>2</sub>O<sub>3</sub>. Notably,  
54 these catalysts are active for the hydrogenation of BA (61-  
55 100%). However, for the hydrogenation of DPBA, the Pd/S-1  
56 and Pd/Al<sub>2</sub>O<sub>3</sub> are still active, but the Pd@S-1 is completely  
57 inactive. This phenomenon is assigned to that the molecule  
58 diameter of DPBA is obviously larger than the size of the S-1  
59 micropores, making the DPBA molecules difficult to access  
60 to the Pd nanoparticles through the microporous channels.  
On the contrary, the Pd/S-1 and Pd/Al<sub>2</sub>O<sub>3</sub> are very active in  
the hydrogenation of DPBA because the Pd nanoparticles are  
directly exposed on the external surface of the catalysts. These  
results confirm that the Pd nanoparticles are fully encapsulated  
inside of the S-1 crystals, forming the Pd@S-1 as a core-shell  
structure.

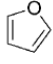
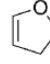
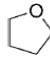
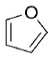
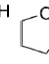
Table 1 presents catalytic data in hydrogenation of furfural  
over the Pd@S-1 and Pd/S-1 in a fixed-bed reactor. The  
major products include furan, dihydrofuran, tetrahydrofuran,  
and furfuryl alcohols. Because furan is a promising platform  
chemical, it is always desirable to get high selectivity in the  
furfural hydrogenation. However, the conventional Pd catalysts  
normally show relatively low selectivity for the furan, which is  
due to the difficulty in the selective cleavage the C-C bond of  
the furfural.<sup>19,25,26</sup> Notably, the Pd@S-1 and Pd/S-1 are very  
active for the furfural hydrogenation, but their furan selectiv-  
ities are quite different (Figure S5). For example, when the  
reaction was carried out at 250 °C, the Pd@S-1 exhibits the  
selectivity for furan as high as 98.7% with furfural conversion  
at 91.3% (entry 5), which is much higher than those of indus-  
trial Pd/Al<sub>2</sub>O<sub>3</sub> catalyst (Table S3) and the catalysts reported  
previously.<sup>19</sup> In this case, it is also detected CO, CO<sub>2</sub>, and  
HCOH formed by C-C cleavage of furfural, Figure S6). In  
contrast, the Pd/S-1 gives similar conversion (91.4%), but  
very low furan selectivity (5.6%, entry 11). In addition, a  
large amount of bulky molecules from the condensation of the  
furfural are detectable (selectivities at 33.7-75.7%, entries  
7-12). Possibly, these bulky molecules could be formed on the  
exposed Pd surface over the Pd/S-1, while these molecules are  
difficult to be formed in the zeolite micropores with sizes of  
~0.55 nm over the Pd@S-1.

Considering that the Pd@S-1 and Pd/S-1 have similar Pd  
loading, nanoparticle size distribution, and the same S-1  
zeolite support, it is reasonably suggested that the high furan  
selectivity over the Pd@S-1 should be directly attributed to the  
core-shell structure rather than other factors. To confirm this  
suggestion, HF treatment of the Pd@S-1 was carried out. After  
partial destroy of the S-1 zeolite framework in the Pd@S-1  
(Figure S7), the treated Pd@S-1-HF gives a significant  
reduction of furan selectivity (46.2%, entry 13), compared  
with the Pd@S-1 (98.7%, entry 5). This result demonstrates  
the importance of the S-1 zeolite as a shell for controlling the  
furan selectivity in the furfural hydrogenation over the Pd@S-1.

The difference in diffusion of reactants and products in the  
hydrogenation was monitored by FT-IR spectra of the adsorbed  
molecules on the Pd@S-1 at first. After desorption under the  
same conditions, the intensity of the band at ~1227 cm<sup>-1</sup>,  
associated with the C-O bond in the furan



**Table 1.** Catalytic data in furfural hydrogenation over various catalysts.<sup>a</sup>

Entry	Catalyst	Temp. (°C)	Conv. (%)	Selectivity (%)						Balance <sup>c</sup>
									Others <sup>b</sup>	
1	Pd@S-1	150	29.1	86.5	3.9	9.6	0	0	0	1.07
2	Pd@S-1	175	50.7	91.8	3.1	5.1	0	0	0	0.98
3	Pd@S-1	200	83.7	95.7	1.4	2.9	0	0	0	0.99
4	Pd@S-1	225	88.9	96.8	1.9	1.3	0	0	0	1.03
5	Pd@S-1	250	91.3	98.7	0.8	0.5	0	0	0	1.03
6	Pd@S-1	275	80.0	77.9	0.3	0.3	0	0	21.5	1.06
7	Pd/S-1	150	43.0	7.0	28.0	20.5	7.0	0	37.5	1.08
8	Pd/S-1	175	44.2	13.5	11.5	31.7	9.6	0	33.7	0.87
9	Pd/S-1	200	63.5	11.3	2.2	18.9	7.6	0	60.0	0.91
10	Pd/S-1	225	89.0	8.1	1.6	11.6	13.2	0	65.5	0.88
11	Pd/S-1	250	91.4	5.6	1.1	12.3	12.7	0	68.3	0.93
12	Pd/S-1	275	96.7	6.9	0	13.2	4.2	0	75.7	1.02
13	Pd@S-1-HF <sup>d</sup>	250	81.0	46.2	0	11.1	40.1	2.6	0	0.98

<sup>a</sup> Reaction condition: 5 wt% furfural (mass ratio of furfural/*n*-butyl alcohol at 1:19), feed rate at 0.5ml/h, 10% H<sub>2</sub>/Ar at a rate of 10 ml/min, 100 mg of catalyst, 1 atm pressure; <sup>b</sup> Bulky molecules from the condensation of furfural; <sup>c</sup> Molecular balance during the reaction, calculated from the amount of furan and tetrahydrofuran rings in feeds and products; <sup>d</sup> The HF-treated Pd@S-1 was used as catalyst.

or tetrahydrofuran rings of these molecules, could be reduced in the Pd@S-1 (Figure S8). By analyzing a change in the band intensity (Table S4), it is calculated the desorption percentage for the 1227 cm<sup>-1</sup> band intensities of various molecules, as summarized in Figure 2A. Clearly, desorption of more molecules means faster molecular diffusion in the S-1 micropores. Interestingly, the desorption percentage of furan (46.6%) is much more than that of furfural, furfuryl alcohol, tetrahydrofuran, tetrahydrofurfuryl alcohol, and methylfuran (3.9–28.9%). These results suggest that the furan has much faster diffusion rate than that of the other molecules in the micropores of the Pd@S-1. Further evidence for faster diffusion rate of the furan than that of the other molecules in the S-1 micropores is given by the temperature programmed desorption (TPD) measurements of these molecules (Figure S9).

Understanding of diffusion behavior of various molecules in the micropores of S-1 zeolite was also performed by theoretical simulation. Figure S10 shows the models of furfural, furan, furfuryl alcohol, tetrahydrofuran, tetrahydrofurfuryl alcohol, and methylfuran localized in the microporous channels of the S-1 zeolite, and their calculated adsorption energies (*E<sub>ads</sub>*) for various molecules are shown in Figure 2B. The *E<sub>ads</sub>* for per furan molecule is -6.06 eV, which has lower absolute value than those of furfural (-6.18 eV), furfuryl alcohol (-9.34 eV), tetrahydrofuran (-7.05 eV), tetrahydrofurfuryl alcohol (-9.75 eV), and methylfuran (-7.05 eV). These results indicate that the zeolite microporous channels tend to adsorb the furan molecule much more weakly than the other molecules, suggesting that the furan molecules tends to diffuse more faster through the zeolite micropores than that of the other molecules, in good agreement with those obtained from IR spectroscopy (Figure S8 and Table S4) and TPD measurements (Figure S9).

Based on these results, it is proposed that, for example, if furfuryl alcohol was formed from the furfural hydrogenation, which is a major side reaction paralleling with the decarbonylation to directly form furan,<sup>19,25</sup> it tends to be localized on the Pd sites by strong adsorption in zeolite micropores, thus leading to further reaction until to form easily diffused furan molecule (Table S5). This proposed mechanism could also be confirmed by the fact that the furfuryl alcohol was

completely undetectable over the Pd@S-1, due to the strong adsorption ability of micropores to this molecule. In contrast, the furfuryl alcohol is always formed over the Pd/S-1 and Pd/Al<sub>2</sub>O<sub>3</sub> catalyst (Tables 1 and S3), because of the lack of zeolite micropores on the Pd surface.

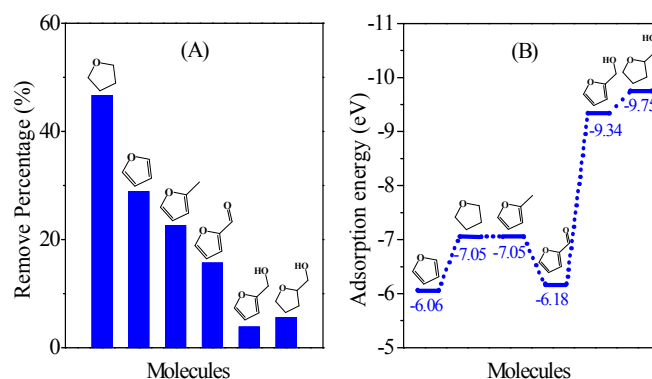


**Figure 2.** (A) The percentage of various molecules removed from Pd@S-1 during the same desorption treatment. (B) Calculated adsorption energy for each molecule in the micropores of the S-1 zeolite.

Figure 3 shows the dependence of furfural conversion and furan selectivity on reaction time over the Pd@S-1. The catalyst retains its activity and selectivity in the period of 8 h, then reduces the furfural conversion. After calcination at 550 °C for 3 h in oxygen flowing, the Pd@S-1 completely regenerated its catalytic property by removing the coke in the catalyst (Figure S11). Even if the reaction time reaches to 60 h, the Pd@S-1 still keeps similar furfural conversion and furan selectivity to the fresh catalyst. TEM image of the Pd@S-1 reacted for 60 h shows that the size distribution of Pd nanoparticles is very similar to those of the fresh catalyst (Figure S12), indicating that high regenerated activity and selectivity should be from good stability of these Pd nanoparticles during the hydrogenated process. Even if calcination of the Pd@S-1 at 600 °C for 4 h in air, the Pd nanoparticles still keep their Pd size distribution (Figure S13). In

comparison, most of the Pd nanoparticles on the external surface of S-1 zeolite aggregate to larger than 10 nm nanoparticles after the same treatment (Figure S14). This phenomenon could be assigned to the unique core-shell structure of Pd@S-1 zeolite, where the S-1 shell prevents the aggregation of Pd nanoparticles.<sup>27-29</sup>

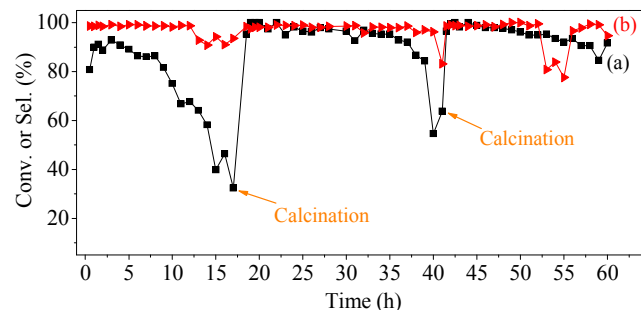


**Figure 3.** Dependence of (a) conversion of furfural and (b) selectivity of furan over the Pd@S-1 in hydrogenation of furfural to furan.

It is worth noting that the strategy of controlling product selectivity by zeolite crystals is not only applied to Pd nanoparticles but also to Ru and Pt nanoparticles. For example, in the selective hydrogenation of furfural to furan, the S-1 zeolite encapsulated Ru and Pt nanoparticles are also synthesized by the solvent-free route (Figures S15 and S16), significantly exhibiting higher furan selectivity than the Ru and Pt nanoparticles on the external surface of S-1 crystals (Tables S6 and S7).

In summary, we show a novel strategy to control the furan selectivity in the furfural hydrogenation over a core-shell structural Pd@S-1 catalyst synthesized from a solvent-free crystallization. This catalyst efficiently combines high activity of the Pd nanoparticles and excellent selectivity of zeolite micropores, giving the furan selectivity as high as 98.7% with furfural conversion at 91.3%. In addition, this catalyst is easily regenerated by calcination at 550 °C. The strategy for preparation of the Pd@S-1 with high activity, excellent selectivity, and superior regenerated activity in the furfural hydrogenation should be potentially important for designing and developing highly efficient heterogeneous catalysts in the future.

## ASSOCIATED CONTENT

### Supporting Information

This material is available free of charge via the Internet at <http://pubs.acs.org>.

## AUTHOR INFORMATION

### Corresponding Author

Email: [liangwang@zju.edu.cn](mailto:liangwang@zju.edu.cn) (L.W.)

Email: [fsxiao@zju.edu.cn](mailto:fsxiao@zju.edu.cn) (F.S.X.)

### Notes

The authors declare no competing financial interest.

## ACKNOWLEDGMENT

This work is supported by National Natural Science Foundation of China (21333009, U1462202, and 21403192).

## REFERENCES

- (1) Zhang, X.; Liu, D.; Xu, D.; Asahina, S.; Cychosz, K. A.; Agrawal, K. V.; Al Wahedi, Y.; Bhan, A.; Al Hashimi, S.; Terasaki, O.; Thommes, M.; Tsapatsis, M. *J. Am. Chem. Soc.* **2012**, *336*, 1684-1687.
- (2) Lew, C. M.; Rajabbeigi, N.; Tsapatsis, M. *Micro. Meso. Mater.* **2012**, *153*, 55-58.
- (3) Chang, C.; Green, S. K.; Williams, C. L.; Dauenhauer, P. J.; Fan, W. *Green Chem.* **2014**, *16*, 585-588.
- (4) Xia, Q.-N.; Cuan, Q.; Liu, X.-H.; Gong, X.-Q.; Lu, G.-Z.; Wang, Y.-Q. *Angew. Chem. Int. Ed.* **2014**, *53*, 9755-9760.
- (5) Su, D. S.; Perathoner, S.; Centi, G. *Chem. Rev.* **2013**, *113*, 5782-5816.
- (6) Román-Leshkov, Y.; Barrett, C. J.; Liu, Z. Y.; Dumesic, J. A. *Nature* **2007**, *447*, 982-986.
- (7) Do, P. T. M.; McAtee, J. R.; Watson, D. A.; Lobo, R. F. *ACS Catal.* **2013**, *3*, 41-46.
- (8) Lam, E.; Luong, J. H. T. *ACS Catal.* **2014**, *4*, 3393-3410.
- (9) Román-Leshkov, Y.; Moliner, M.; Labinger, J. A.; Davis, M. E. *Angew. Chem. Int. Ed.* **2010**, *49*, 8954-8957.
- (10) Yang, J.; Li, N.; Li, S.; Wang, W.; Li, L.; Wang, A.; Wang, X.; Cong, Y.; Zhang, T. *Green Chem.* **2014**, *16*, 4879-4884.
- (11) Corma, A.; Iborra, S.; Velty, A. *Chem. Rev.* **2007**, *107*, 2411-2502.
- (12) Liu, D. J.; Chen, E. Y.-X. *ACS Catal.* **2014**, *4*, 1302-1310.
- (13) Chheda, J. N.; Huber, G. W.; Dumesic, J. A. *Angew. Chem. Int. Ed.* **2007**, *46*, 7164-7183.
- (14) Wang, H. M.; Male, J.; Wang, Y. *ACS Catal.* **2013**, *3*, 1047-1070.
- (15) Peng, B.; Yao, Y.; Zhao, C.; Lercher, J. A. *Angew. Chem. Int. Ed.* **2012**, *51*, 2072-2075.
- (16) Corma, A.; Iborra, S.; Velty, A. *Chem. Rev.* **2007**, *107*, 2411-2502.
- (17) Schrader, I.; Warneke, J.; Backenkohler, J.; Kunz, S. *J. Am. Chem. Soc.* **2015**, *137*, 905-912.
- (18) Pang, S. H.; Schoenbaum, C. A.; Schwartz, D. K.; Medlin, J. W. *Nat. Commun.* **2013**, *4*, 2448.
- (19) Zhang, H.; Gu, X.-K.; Canlas, C.; Kropf, A. J.; Aich, P.; Greeley, J. P.; Elam, J. W.; Meyers, R. J.; Dumesic, J. A.; Stair, P. C.; Marshall, C. L. *Angew. Chem. Int. Ed.* **2014**, *53*, 12132-12136.
- (20) Ma, X.; Zhou, A.; Song, C. *Catal. Today* **2007**, *123*, 276-284.
- (21) Liu, F.; Willhammar, T.; Wang, L.; Zhu, L.; Sun, Q.; Meng, X.; Carrillo-Cabrera, W.; Zou, X.; Xiao, F.-S. *J. Am. Chem. Soc.* **2012**, *134*, 4557-4560.
- (22) Dai, C.; Zhang, A.; Liu, M.; Guo, X.; Song, C. *Adv. Funct. Mater.* **2015**, *25*, 7479-7487.
- (23) Liu, F.; Wang, L.; Sun, Q.; Zhu, L.; Meng, X.; Xiao, F.-S. *J. Am. Chem. Soc.* **2012**, *134*, 16948-16950.
- (24) Ren, L.; Wu, Q.; Yang, C.; Zhu, L.; Li, C.; Zhang, P.; Zhang, H.; Meng, X.; Xiao, F.-S. *J. Am. Chem. Soc.* **2012**, *134*, 15173-15176.
- (25) Bhogswararao, S.; Srinivas, D. *J. Catal.* **2015**, *327*, 65-77.
- (26) Simon, H. P.; Carolyn, A. S.; Daniel, K. S.; J, W. M. *ACS Catal.* **2014**, *4*, 3123-3131.
- (27) Laursen, A. B.; Højholt, K. T.; Lundegaard, L. F.; Simonsen, S. B.; Helveg, S.; Schuth, F.; Paul, M.; Grunwaldt, J.-D.; Kegncs, S.; Christensen, C. H.; Egeblad, K. *Angew. Chem. Int. Ed.* **2010**, *49*, 3504-3507.
- (28) Goel, S.; Zones, S. I.; Iglesia, E. *J. Am. Chem. Soc.* **2014**, *136*, 15280-15290.
- (29) Mielby, J.; Abildstrøm, J. O.; Wang, F.; Kasama, T.; Weidenthaler, C.; Kegncs, S. *Angew. Chem. Int. Ed.* **2014**, *53*, 1-5.

